Adsorption of C_1-C_7 Normal Alkanes on BAX Activated Carbon. 1. Potential Theory Correlation and Adsorbent Characterization

Charles E. Holland, Shaheen A. Al-Muhtaseb, and James A. Ritter*

Department of Chemical Engineering, College of Engineering and Information Technology, Swearingen Engineering Center, University of South Carolina, Columbia, South Carolina 29208

Single-component adsorption equilibria of the *n*-alkane series C_1-C_7 on Westvaco BAX-1100 activated carbon were measured over very broad ranges of temperature and pressure, spanning 293−393 K and 0.06−4964 Torr, depending on the *n*-alkane. The 4278 data points were correlated successfully with potential theory and collapsed essentially into one characteristic curve. A useful functional form of the characteristic curve was also obtained. A new potential theory approach, based on a multisegment Gaussian distribution, qualitatively predicted both the pore size distribution and the total pore volume of the BAX-1100 activated carbon from the adsorption equilibria of the C_3-C_7 *n*-alkanes, with errors in the total pore volume ranging between 1 and 5%. This extensive data set should prove to be very useful for testing adsorbent characterization schemes, evaluating adsorption isotherm models, estimating adsorption thermodynamic properties of these systems, and modeling adsorption processes concerning hydrocarbon separations and purification, in general.

Introduction

The measurement of single-component adsorption equilibria over a relatively wide range of experimental conditions has many different uses. It is extremely useful for characterizing different adsorbent surfaces and investigating the nature of their interactions with the adsorbate molecules.[1−4] It is also useful for evaluating the ability of different models to correlate the data over a wide range of conditions. Reliable correlations are also essential for estimating the dependence of different thermodynamic properties of the adsorbed phase on the adsorption conditions,[1−9] and they are useful for simulating cyclic adsorption processes, such as temperature and pressure swing adsorption processes, because the process conditions vary widely during cycling.

However, single-component adsorption equilibria measured over wide ranges of pressure and temperature on commercially available adsorbents are quite rare in the literature. Much of the data that is available is either obsolete because the adsorbent is not being manufactured[10−12] or measured over a relatively narrow range of experimental conditions with only a few data points obtained. For this reason, many of the models in the literature may not be reliable when extrapolated over a broad range of conditions, such as those encountered in cyclic adsorption processes. Therefore, the major objective of this work is to present an extensive set of single-component adsorption isotherm data that can be used for adsorbent characterization, model evaluation, thermodynamic property estimation, and process modeling.

In Part 1 of this series, the single-component adsorption equilibria for the *n*-alkane series C_1-C_7 measured on Westvaco BAX-1100 activated carbon over a wide range of conditions are presented, along with a characteristic curve predicted from potential theory. A new potential theory approach is also presented for predicting the pore size distribution (PSD) and the total pore volume of the BAX-1100 activated carbon. It is applied to the experimental data for each adsorbate, and the results are compared with predictions based on density functional theory[13] and another potential theory approach in the literature.[14−29] In Part 2 of this series, all of the adsorption equilibria are utilized to study the ability of different pressure-explicit isotherm models to represent the data. These models are then used to predict the isosteric heats of adsorption and the adsorbed-phase heat capacities of the *n*-alkane series on BAX-1100 activated carbon.

Theory

The potential theory model has been used extensively for correlating adsorption equilibria on porous adsorbents.[14−17] It has been most successful at uniting the adsorption equilibria for one adsorbent into a single characteristic curve that accounts for the effects of temperature and, when an empirical coalescing factor (β) is used,[15] the polar interactions between the adsorbent and different adsorbates. One of the more common expressions for the characteristic curve is

$$nv = f\left(\frac{A}{\beta v}\right) \tag{1}$$

where the adsorption potential, A, is given by

$$A = RT\ln(P_r^{-1}) = RT\ln\left(\frac{P^0}{P}\right) \tag{2}$$

and n is the amount adsorbed; R is the universal gas constant; T is the temperature; P_r ($= P/P^0$) is the relative pressure; P and P^0 are the equilibrium pressure and vapor pressure of the adsorbate, respectively, at temperature T; and β is the coalescing factor. v, the molar volume of the adsorbed phase, has been estimated in

* Author to whom correspondence should be addressed. Phone: (803) 777-3590. Fax: (803) 777-8265. E-mail: ritter@engr.sc.edu.

10.1021/ie0004794 CCC: $20.00
Published on Web 11/18/2000

various ways in the literature.[15,16] It is estimated here from the molar volume of the adsorbate in the liquid phase at its normal boiling point temperature. Other alternative forms of the adsorption potential have also been explored[14−17] but are not considered here.

The potential theory has also been utilized for characterizing porous adsorbents[18−29] and even for predicting pore size distributions.[18,20−23] The most common and fundamental technique is based on the original form of Dubinin's potential theory for microporous adsorbents[18,20]

$$W' = W_0 \exp\left[-\left(\frac{A}{\beta E_0}\right)^2\right] \tag{3}$$

where W' is the total volume adsorbed ($= nv$), W_0 is the total pore volume, E_0 is the energy of adsorption, and A and β are as previously defined. An empirical dependence between E_0 and the pore width, x, is given by[20,21,23,25,28]

$$E_0 = 2k/x \tag{4}$$

where k is an empirical constant that varies slightly with the nature of the adsorbent.[21] In most cases, however, k has been found to be approximately equal to 120 kJ Å/mole, which is the value used in this work.

Equations 3 and 4 have been extended for predicting the pore size distribution by assuming a PSD function, $f(x)$, and then using it to obtain the overall adsorption isotherm according to

$$W = \int_0^\infty W' f(x)\, \mathrm{d}x \tag{5}$$

where W' now represents the volume adsorbed in a pore of width x. The most commonly used form of $f(x)$ has been the Gaussian distribution defined in terms of pore width,[20] which is written as

$$f(x) = \frac{1}{\delta\sqrt{2\pi}} \exp\left[-\frac{1}{2}\left(\frac{x_0 - x}{\delta}\right)^2\right] \tag{6}$$

where δ and x_0 are the dispersion term and mean pore width, respectively. Substituting eqs 3, 4, and 6 into eq 5 gives the Dubinin−Stoeckli (DS)[20] adsorption isotherm as

$$W = \frac{W_0}{2\sqrt{1 + 2m\delta^2A^2}} \exp\left[-\frac{mx_0^2A^2}{1 + 2m\delta^2A^2}\right]\left[1 + \mathrm{erf}\left(\frac{x_0}{\delta\sqrt{2}\sqrt{1 + 2m\delta^2A^2}}\right)\right] \tag{7}$$

where $m = (1/2\beta k)^2$. This equation, and other forms of potential theory modified for heterogeneous adsorbents, has been reported to be reliable only for low relative pressures.[18,23] Therefore, a new approach is taken in this study wherein a multisegment version of eq 7 is used to account for relative pressures (P_r) in the overall range between zero and one.

This new approach requires that the overall range of P_r be divided into several segments and that the adsorption isotherm data in each segment be fitted independently according to eq 7. The resulting overlapping pore size distributions are then cut off at their points of intersection, which produces an essentially continuous PSD from the discrete PSDs. The total pore volume is then obtained by averaging according to

$$W_{0t} = \frac{\sum_{j=\text{segment 1}}^{J} p_j W_{0j}}{\sum_{j=\text{segment 1}}^{J} p_j} \tag{8}$$

where J is the total number of relative pressure segments applied to the adsorption isotherm data; W_{0j} is the fitted pore size volume, W_0, for P_r segment j; and p_j is a weighing factor that represents the relative significance of the pore volume utilized in segment j to the total pore volume. An expression for p_j was obtained empirically from the probability of occurrence of pore sizes in segment j relative to the overall PSD. This relative probability is estimated from

$$p_j = \frac{\int_{x_{j-1}}^{x_j} f_j(x)\, \mathrm{d}x}{\int_0^\infty f_j(x)\, \mathrm{d}x} \tag{9a}$$

where x_{j-1} and x_j are the lower and upper cutoff limits, respectively, for the PSD of P_r segment j with $x_0 = 0$ and $x_{NJ} = \infty$. NJ is the total number of pressure segments. $f_j(x)$ is the PSD function of increment j and given by eq 6 in terms of the parameters x_{0j} and δ_j, which are the fitted values of x_0 and δ for segment j. Substituting eq 6 for segment j into eq 9a and simplifying leads to

$$p_j = \left[\mathrm{erf}\left(\frac{x_j - x_{0j}}{\sqrt{2}\delta_j}\right) - \mathrm{erf}\left(\frac{x_{j-1} - x_{0j}}{\sqrt{2}\delta_j}\right)\right] \Big/ \left[1 + \mathrm{erf}\left(\frac{x_{0j}}{\sqrt{2}\delta_j}\right)\right] \tag{9b}$$

In contrast, the total pore volume predicted from the one-segment approach results in a total pore volume of $W_{0t} = W_0$.

Experimental Section

Materials. CP-grade helium, methane, ethane, and *n*-butane were obtained from National Welders. CP-grade propane was obtained from Matheson Gas Products, Inc. *n*-Pentane and *n*-heptane were >99% pure and were obtained from Alfa AESAR, and *n*-hexane was >99% pure and was obtained from Sigma Chemicals Company. All of these adsorbates were used as received. The BAX-1100 activated carbon was obtained from Westvaco in the form of pellets (2.1 mm extruded) and used as received, except for regeneration.

Adsorption Equilibria Measurement and Adsorbent Characterization. Adsorption equilibria for methane, ethane, propane, *n*-butane, *n*-pentane, *n*-hexane and *n*-heptane on BAX-1100 activated carbon were measured gravimetrically using a VTI integrated microbalance system driven with in-house-developed National Instruments LabView hardware and software. Typically, 80−150 mg of activated carbon were loaded into the system, depending on the *n*-alkane being investigated. Prior to each isotherm measurement, the activated carbon was regenerated at 523 K for 2 h under a vacuum of less than 1×10^{-5} Torr. Precision was confirmed by carrying out multiple runs with different

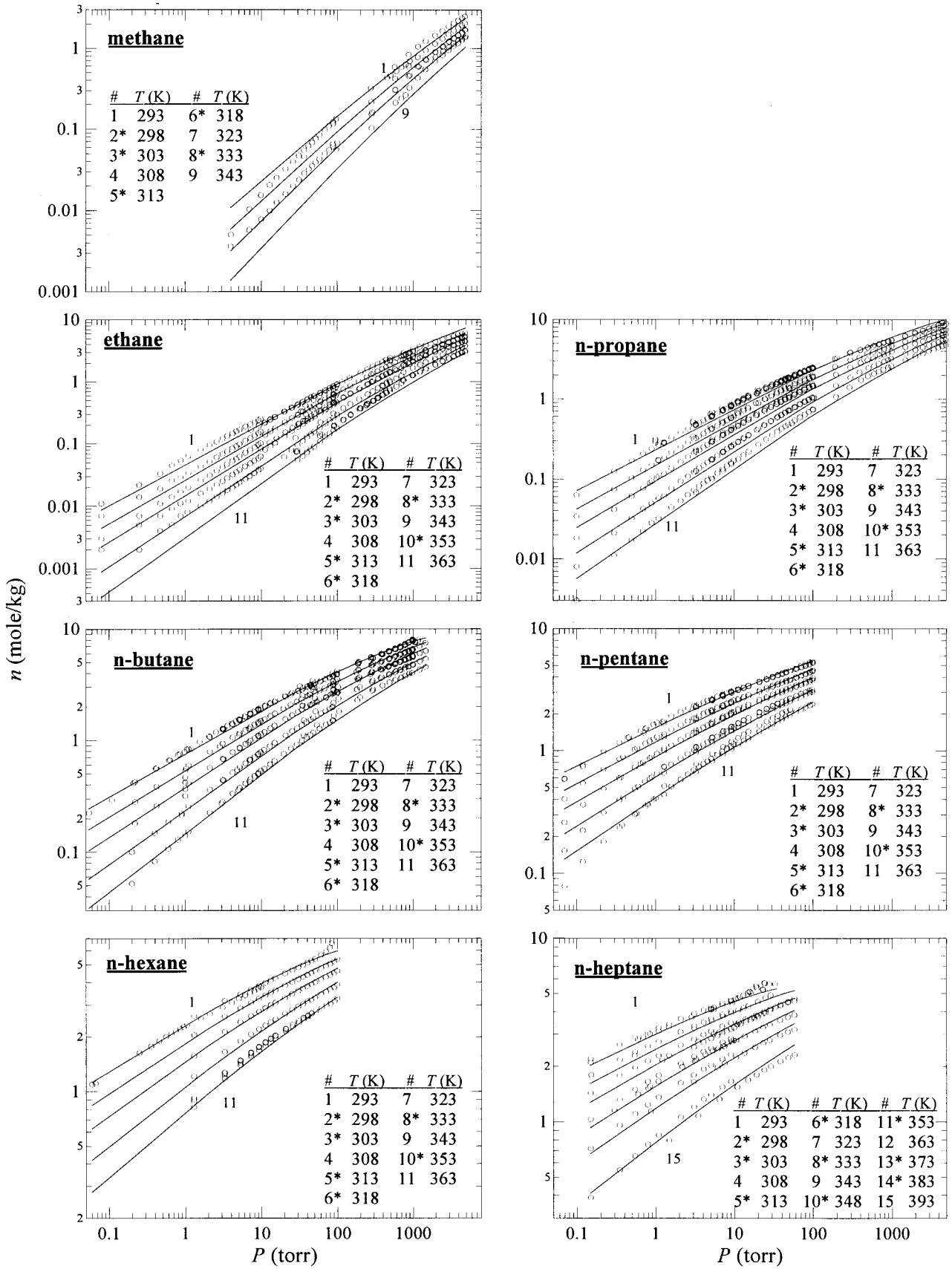

Figure 1. Adsorption equilibria of the normal alkane series C_1-C_7 on BAX-1100 activated carbon. Symbols represent experimental data, and lines represent predictions from eq 12, the potential theory characteristic curve correlation (Figure 2). Asterisks denote isotherms measured but not plotted here for clarity.

adsorbent samples and repeated runs with the same sample; virtually identical results were obtained in all cases. Accuracy was confirmed by reproducing an *n*-butane isotherm on BAX-1100 activated carbon at 298 K that was supplied by Westvaco; when plotted, the two isotherms were indistinguishable. Also, buoyancy cor-

Table 1. Ranges of Experimental Conditions for the Adsorption Equilibria of the *n*-Alkane Series C_1-C_7 on BAX-1100 Activated Carbon and Some Thermodynamic Parameters of the Adsorbates

alkane	N_p	P (Torr)	T (K)	ζ (cm³/mole)	T_{nbp} (K)	T_c (K)
C_1	181	3.96−4964	293−343	7.343	111.67	647.28
C_2	823	0.08−4948	293−363	7.882	184.56	305.56
C_3	897	0.10−4953	293−363	10.348	231.11	369.94
n-C_4	869	0.06−1494	293−363	12.994	272.67	425.17
n-C_5	812	0.07−100	293−363	15.268	309.22	469.78
n-C_6	323	0.06−100	293−363	17.638	341.89	507.89
n-C_7	373	0.15- 58	293−393	20.052	371.61	540.17

rections were measured with helium over the full ranges of temperature and pressure studied for each of the *n*-alkanes and for the largest loading of activated carbon used. In all cases, after corrections for molecular weight were performed, the bouyancy corrections were found to be negligible.

The pore size distribution, total pore volume, and BET surface area of the Westvaco BAX-1100 activated carbon were measured with nitrogen at 77 K using Micromeritics ASAP2010 hardware and software. For both accuracy and precision, the system required a sample size corresponding to 50−100 m^2 of adsorbent surface area; thus, around 60 mg of activated carbon were characterized in each measurement. The activated carbon was regenerated in situ in an ultrasonically cleaned and dried sample tube at 473 K for 24 h under a vacuum of less than 1×10^{-6} Torr. Precision was confirmed by carrying out multiple runs with different adsorbent samples and repeated runs with the same sample; again, virtually identical results were obtained in all runs. Accuracy was confirmed by reproducing a nitrogen isotherm on BAX-1100 activated carbon at 77 K that was supplied by Westvaco; again, when plotted, the two isotherms were indistinguishable.

Results and Discussion

Potential Theory Correlation. The experimental adsorption equilibria of the C_1-C_7 *n*-alkane series on BAX-1100 activated carbon are summarized in Table 1. Temperatures ranged from 293 to 393 K, pressures ranged from 0.06 to 4964 Torr, and the number of data points ranged from 181 to 897, depending on the *n*-alkane. The complete set of tabulated data is available in an electronic (Microsoft Excel) format from the corresponding author or as Supporting Information. Representative experimental adsorption isotherms for each *n*-alkane are displayed in Figure 1 by symbols.

Figure 2 displays the characteristic curve obtained by correlating all of the experimental adsorption equilibria with the potential theory model described by eqs 1 and 2. The coalescing factors, β, were optimized geometrically in reference to ethane, which was given the reference β of 1. The resulting values are listed in Figure 2. Notice that, in general, β decreased with increasing carbon number; however, no specific trend was observed that allowed β to be correlated with the carbon number. This characteristic curve was fitted to A using the least sum square error (LSSE) method in the logarithm of the total volume of the adsorbed phase, $\ln(nv)$, according to the following objective function:

$$F' = \min\left(\sum_{N=1}^{7}\left[\sum_{i=1}^{N_P}[\ln(vn^{corr}) - \ln(vn^{exp})]_i^2\right]_{C_N}\right) \quad (10)$$

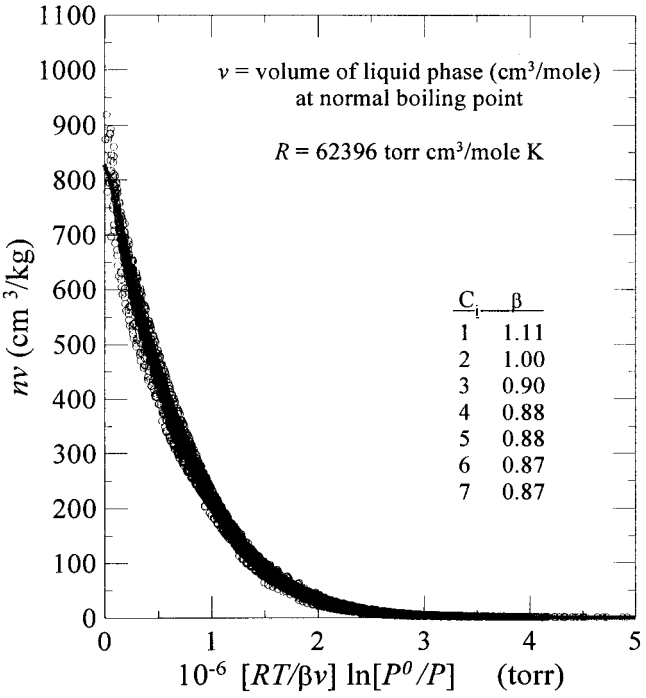

Figure 2. Potential theory characteristic curve obtained from the adsorption equilibria of the *n*-alkane series C_1-C_7 on BAX-1100 activated carbon. Symbols represent experimental data, and the line represents the best fit to eq 12.

where N is the number of carbon atoms in the *n*-alkane molecule. v was obtained from the following correlation[30] for the specific volume of the liquid phase in terms of temperature:

$$v = \zeta(5.7 + 3T_{nbp}/T_c) \quad (11)$$

where T_{nbp} is the normal boiling point temperature, T_c is the critical temperature, and ζ is a temperature-independent correlation constant.[30] T_{nbp}, T_c, and ζ were obtained from the literature[30] and are listed in Table 1. The best (yet simplest) correlation for describing the characteristic curve was taken as a two-term power formula of $\ln(nv)$, which gives

$$nv = 825.421 \times \exp\left[-6.85858 \times 10^{-8}\left(\frac{A}{\beta v}\right)^{1.218}\right] \quad (12)$$

where A and v are obtained from eqs 2 and 11, respectively. The value of R used in this work to calculate A from eq 2 was 62396 Torr cm^3 mol^{-1} K^{-1}, T is in Kelvin, and n is in moles adsorbed per kilogram of adsorbent. Correlations from eq 12 are also plotted in Figure 1 (lines). They show reasonable agreement with the representative experimental data (symbols) for all of the alkanes. The average relative error, *ARE* (estimated from eq 13), in the amounts adsorbed predicted from eq 12 for the entire *n*-alkane series was 7.18%.

$$ARE(\%) = \frac{100}{\sum_{N=1}^{7} N_{P,C_N}}\sum_{N=1}^{7}\left(\sum_{i=1}^{N_P}\frac{|n^{corr} - n^{exp}|}{n^{exp}}\right)_{C_N} \quad (13)$$

This low value of the overall *ARE* indicates that eq 12 satisfactorily represents the whole system of adsorption equilibria; therefore, this potential theory correlation is quite accurate over a broad range of experimental

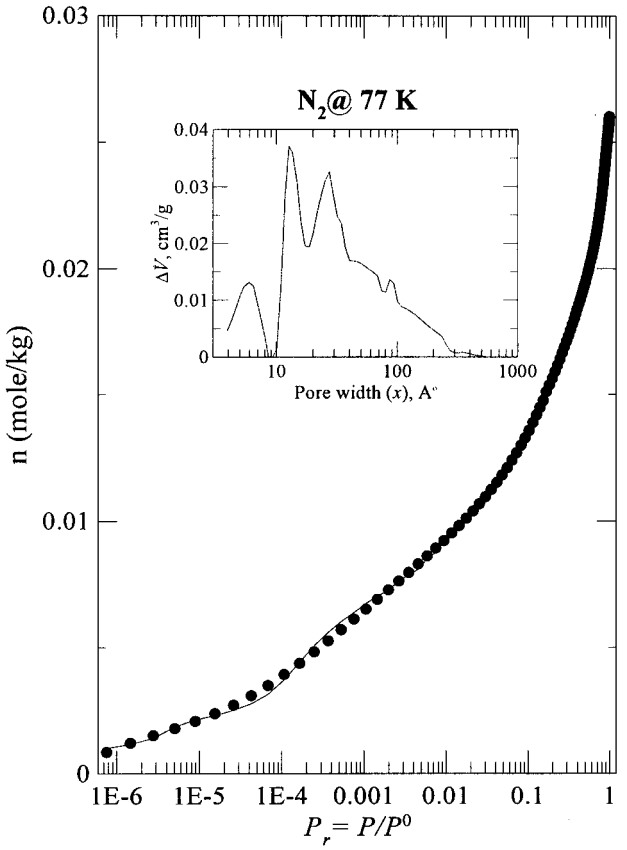

Figure 3. Nitrogen adsorption isotherm on BAX-1100 activated carbon at 77 K. Symbols represent experimental data, and the line represents the prediction from DFT. Inset: Corresponding pore volume distribution predicted from a DFT analysis.

conditions for the *n*-alkane series C_1-C_7 adsorbed on BAX-1100 activated carbon.

Predicted Pore Size Distributions. The pore size distribution obtained from the ASAP2010 via a DFT analysis is shown in Figure 3, along with the experimental nitrogen isotherm (symbols) and the corresponding fit to this isotherm with DFT (solid lines). The ASAP2010 provides a standard software package for estimating the PSD from the measured adsorption equilibria via a DFT method. This software has only one input parameter, the regularization parameter (RP), which can be set to one of four values: none, low, medium, and high. It is noteworthy that the low, medium, and high values all gave nearly identical results (not shown) in both the predicted adsorption isotherm and the resulting PSD, which added confidence to the convergence of the optimization method. The results in Figure 3 correspond to the medium value of RP, and they show that the DFT method was capable of reproducing the nitrogen isotherm extremely well, which lends credence to the PSD obtained in this manner. This PSD exhibits three distinct peaks at about 6, 12, and 25 Å, whereas a broad shoulder begins at about 40 Å and extends to about 300 Å, the upper limit of the applicability of the DFT method. Also, the smallest pores identified by nitrogen filling are about 4 Å, in agreement with the molecular diameter of nitrogen being about 3.7 Å, as estimated from the Lennard-Jones parameter (σ).[31] Therefore, BAX-1100 activated carbon contains a fair amount of structural heterogeneity within a multinodal distribution of pore sizes and with a large fraction of the pore volume associated with mesopores. The total pore volume and BET surface area of the BAX-1100 activated carbon were also obtained from the ASAP2010 analysis as 0.799 cm^3/g and 1251 m^2/g, respectively. With the PSD predicted satisfactorily from DFT, and accepting the fact that this state-of-the-art technique produces the best possible estimate of the actual PSD of the BAX-1100 activated carbon, the DFT PSD was used to evaluate the creditability of the different alkane adsorption isotherms to provide an approximation of the PSD by applying the isotherms to different potential theory PSD prediction methods.

Three different potential theory approaches were examined for predicting the PSD of the BAX-1100 activated carbon from the experimental adsorption equilibria for each adsorbate in the *n*-alkane series C_1-C_7. The first two approaches adopted in this work were based on the popular, one-segment Gaussian distribution that leads to the DS potential theory equation.[20] However, the DS and other similar models were reported to be reliable only in the low range of relative pressures for predicting the PSD.[18,23] Therefore, to further examine this reliability, the one-segment approach was applied in this work with P_r limits of both 0.3 and 1.0. The third approach corresponds to the multisegment Gaussian distribution approach discussed earlier. Note that, because the objective here was to evaluate each adsorbate independently from the other adsorbates, β was set to unity for each of the *n*-alkanes for all three potential theory approaches.

For the multisegment approach, five segments were found to be efficient for fitting the extensive experimental data set presented in this work. Thus, the experimental data were divided into five segments, numbered with roman numerals *i* through *v*, with P_r ranges of (*i*) 0−0.005, (*ii*) 0.005−0.03, (*iii*) 0.03−0.1, (*iv*) 0.1−0.6 and (*v*) 0.6−1.0, whenever these ranges existed within the experimental data set. Values of *A* were recalculated with $R = 8.314$ J mol^{-1} K^{-1}, and the adsorption equilibria in each segment were fitted independently to eq 7 by minimizing the following objective function for each of the *n*-alkanes:

$$F = \min\left[\sum_{i=1}^{N_{Pj}} (\ln W_i^{\exp} - \ln W_i^{\text{calc}})^2\right]_j \qquad (14)$$

where *j* is the P_r segment number, N_{Pj} is the number of experimental data points within segment *j*, $W_i^{\exp} = n^{\exp} \times v$, $n^{\exp}$ is the experimental amount adsorbed, and W_i^{calc} is the correlated adsorbed-phase volume estimated from eq 7. The corresponding *ARE* values, estimated from eq 15 (with N_{Pj} instead of N_P), and the optimum fitting parameters are shown in Table 2.

$$ARE(\%) = \frac{100}{N_{Pj}} \sum_{i=1}^{N_{Pj}} \frac{|n^{\exp} - n^{\text{corr}}|}{n^{\exp}} \qquad (15)$$

In accordance with Dubinin's approach,[20] the pore volume distribution in terms of pore sizes is given by $W_0 \times f(x)$, where W_0 is the fitted total pore volume and $f(x)$ is calculated from eq 6 with the fitted values of x_0 and δ. Similar analyses were carried out for the two one-segment approaches but with P_r ranges fixed from 0−0.3 and 0−1.0; thus, $j = 1$ in both cases, and only the *ARE* values are reported in Table 2. It was not surprising that the *ARE* values were, in general, much higher for the one-segment approaches compared to the multisegment approach. The PSDs obtained from the multiseg-

Table 2. DS Potential Theory Correlation Parameters and Corresponding *ARE* Values Obtained from Fitting the Adsorption Equilibria of the *n*-Alkane Series C_1−C_7 on BAX-1100 Activated Carbon to the New Multisegment and the Original One-Segment Gaussian Pore Size Distribution Models

P_r segment	parameter	C_1	C_2	C_3	C_4	C_5	C_6	C_7
	W_0 (cm³/kg)	297.6	296.3	330.7	426.2	480.4	522.3	590.2
i	x_0 (Å)	27.166	24.122	19.557	17.860	15.663	14.555	13.454
$0 < P_r < 0.005$	δ (Å)	4.115	4.577	2.789	3.232	2.414	3.414	3.311
	ARE (%)	14.55	8.53	4.61	1.81	3.08	2.61	3.76
	W_0 (cm³/kg)	378.4	472.2	496.7	532.4	584.5	621.7	779.8
ii	x_0 (Å)	30.102	29.518	23.657	20.189	18.197	16.526	16.783
$0.005 < P_r < 0.03$	δ (Å)	7.718	9.221	6.164	5.839	6.527	7.709	9.757
	ARE (%)	4.02	5.71	2.20	2.58	1.98	2.16	4.24
	W_0 (cm³/kg)	NA[c]	561.8	590.1	1507.3	905.6	1534.8	943.7
iii	x_0 (Å)		32.936	26.616	0.000	16.993	0.000	15.056
$0.03 < P_r < 0.10$	δ (Å)		17.585	14.183	40.820	20.727	30.502	16.387
	ARE (%)		1.76	0.91	1.98	0.98	1.56	3.09
	W_0 (cm³/kg)	NA[c]	512.6	1285.4	*a*	*a*	*a*	*a*,*b*
iv	x_0 (Å)		30.912	0.000				
$0.10 < P_r < 0.60$	δ (Å)		15.577	44.841				
	ARE (%)		0.50	2.29				
	W_0 (cm³/kg)	NA[c]	NA[c]	1502.4	1586.2	NA[c]	2228.7	1770.3
v	x_0 (Å)			0.000	0.000		0.000	0.000
$0.60 < P_r < 1.00$	δ (Å)			84.106	32.472		146.494	44.365
	ARE (%)			1.90	2.03		0.00	2.69
	W_0 (cm³/kg)	574.8	408.3	459.4	597.5	601.9	686.9	684.6
one-segment	x_0 (Å)	29.515	25.818	21.706	20.494	17.732	18.078	15.666
$0.0 < P_r < 0.30$	δ (Å)	4.522	5.094	3.860	4.767	4.121	8.432	6.060
	ARE (%)	15.44	7.83	5.43	5.19	3.75	2.86	4.82
	W_0 (cm³/kg)	same	same	496.1	639.7	same	750.6	743.7
one-segment	x_0 (Å)	(max $P_r < 0.3$)	(max $P_r < 0.3$)	22.316	21.289	(max $P_r < 0.3$)	19.069	16.918
$0.0 < P_r < 1.00$	δ (Å)			4.156	5.256		11.032	7.756
	ARE (%)			6.53	6.10		3.49	5.48

[a] Heavy alkanes exhibit the same behavior in segments *iii* and *iv*; thus, segment *iii* is extended to also cover segment *iv*. [b] Segment *v* for *n*-heptane starts at $P_r = 0.5$ instead of 0.6. [c] NA = No available experimental data in the corresponding segment.

ment approach (thin solid lines) and from the one-segment approaches are displayed in Figure 4 (dashed and dash-dotted lines) for each of the *n*-alkanes. For comparison, the PSD obtained from DFT is also displayed in each of the panels in Figure 4 (thick solid lines).

In all cases, the one-segment models predicted nearly identical trends, independent of the P_r range. For example, the smaller alkanes were qualitatively more descriptive of the PSD in the mesopore region, the widths of the PSDs increased with increasing carbon number in the *n*-alkane series, and the average pore sizes decreased with increasing carbon number in the *n*-alkane series from about 30 Å to about 15 Å. Moreover, as the widths increased, the one-segment Gaussian distributions began to capture more of the multinodal PSD obtained from DFT; however, up to *n*-pentane, pores less than 10 Å in diameter and greater than 30 Å in diameter were not predicted. For *n*-hexane and *n*-heptane, the widths of the PSDs increased so much that they severely overpredicted the distribution of pores less than 10 Å but still did not capture those greater than 35 Å. In contrast, the multisegment approach produced more skewed but essentially continuous distributions (thin solid lines) by truncating each distribution at the meeting point with the subsequent segment. Like the one-segment models, these multisegment distributions widened and shifted to smaller pores with increasing carbon number in the *n*-alkane series. Again, up to *n*-pentane, pores less than 10 Å were not predicted. However, the multisegment model increasingly captured more of the mesopore size distributions, and for *n*-hexane and *n*-heptane, the PSDs agreed at least qualitatively with that obtained from DFT, capturing both the smaller micropores and some of the larger mesopores.

Another alternative approach was to truncate only the $f(x)$ curves (without multiplying them in each segment by the corresponding W_0 value). This resulted in the continuous pore size distributions shown in Figure 5. The resulting cutoff pore sizes from these two multisegment approaches deviated only slightly from each other, as shown in Table 3. The total (cumulative) pore volumes were calculated from eq 8 with the segment number replacing J. Table 3 shows the relative errors in these total pore volumes predicted from both multisegment approaches and the corresponding truncation limits of P_r. Table 3 also gives the relative errors in the total pore volumes predicted from the W_0 values obtained from the one-segment approaches with the experimental adsorption isotherms truncated at $P_r = 0.3$ and $P_r = 1.0$. Clearly, the adsorption equilibria of the larger *n*-alkanes fitted with any of the different potential theory models provided more accurate predictions of the total pore volume. However, a significant improvement in the accuracy was obtained when the multisegment approach was used with the adsorption equilibria truncated at the proper pressure limits. Also, the predictions with the cutoff pore sizes determined from the continuity of the pore size distributions, $f(x)$, were more accurate than those determined with the cutoff pore sizes determined from the continuity of the adsorbed-phase volume distributions, $W_0 \times f(x)$. Moreover, although the predicted pore volumes from the smaller alkane molecules were acceptably close to the experimental values, no reliable limit of relative pressures was clearly observed for pore filling. In other words, it appeared that C_1 and C_2 did not condense and

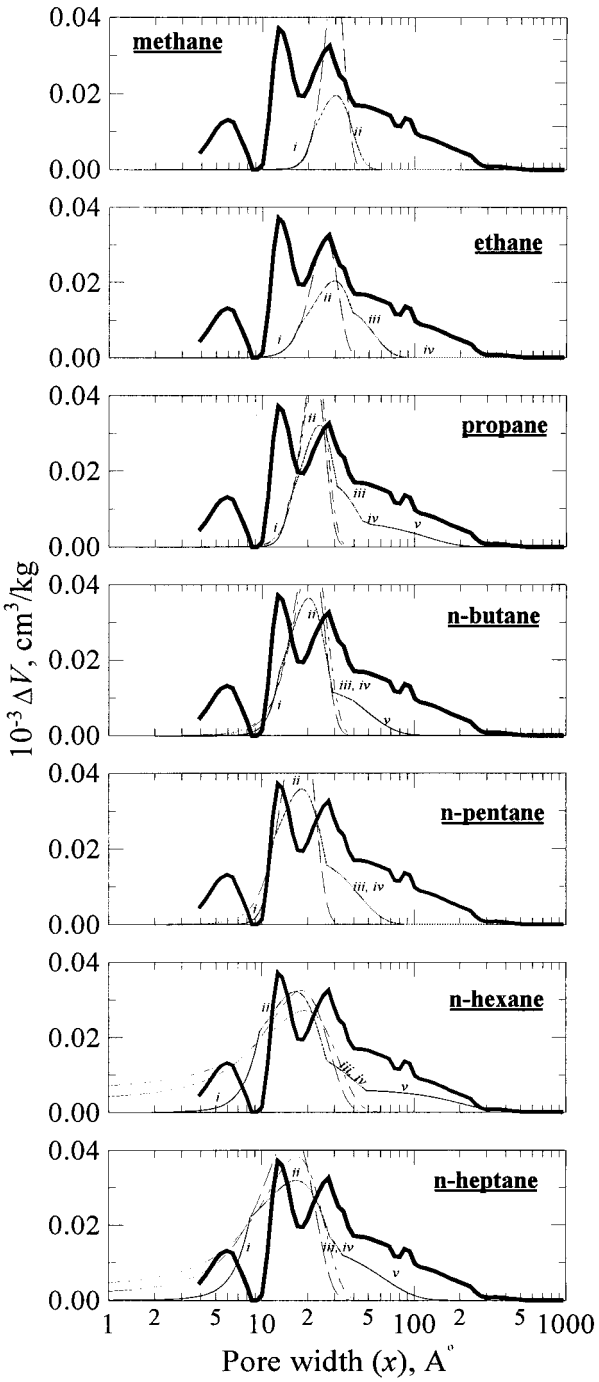

Figure 4. Comparison of pore volume distributions of the BAX-1100 activated carbon obtained from DFT (thick solid line) and predicted from the new multisegment model (thin solid line) and the two original one-segment models with upper P_r limits of 0.3 (dashed lines) and 1.0 (dash−dot lines) for each of the *n*-alkanes.

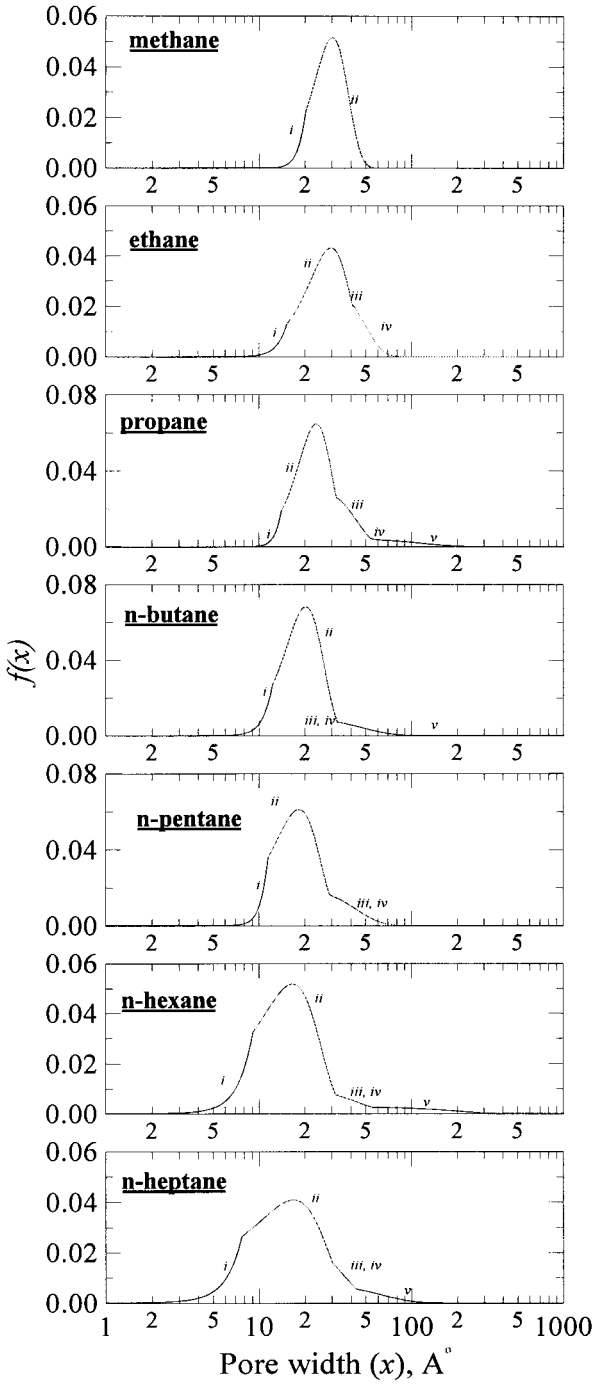

Figure 5. Pore size distributions predicted from the new multisegment model for each of the *n*-alkanes adsorbed on BAX-1100 activated carbon.

thus did not fill the total pore volume over the pressure ranges studied. This was not the case, however, for the heavier alkanes.

Propane clearly exhibited a pore-filling relative pressure within the P_r range investigated, as evidenced by the total volume being within 2% of the experimental value. Moreover, a simple investigation of the pore-filling relative pressures for components heavier than C_3, for which sufficient data were available, revealed that the total pore volume was most accurately predicted at relative pressures of 1, 0.6, and 0.5 for C_4, C_6, and C_7, respectively. Experimental data for C_5 were measured only up to a maximum relative pressure of approximately 0.24. Therefore, although the latter investigation could not be conducted on the C_5 adsorption isotherms, it is expected that the most accurate prediction of the total pore volume with the proposed method would be exhibited at a relative pressure between 0.6 and 1. These relative pressure limits were understood to correspond roughly to the pore-filling or condensation limits of these adsorbates. The error in predicting the total pore volume under these conditions was, in most cases, around or below 1% of the experimental value, as shown in Table 3.

Overall, these results suggest that the potential theory methods should be used with caution for predicting the PSD of an adsorbent. For example, the results

Table 3. Truncation Limits[a] for the Multisegment Gaussian Pore Size Distributions and Average Relative Errors[b] in the Corresponding Total Pore Volumes Predicted from the Adsorption Equilibria of the *n*-Alkane Series C_1−C_7 on BAX-1100 Activated Carbon

	C_1	C_2	C_3	C_4	C_5	C_6	C_7
x_0 (Å)	0.00	0.00	0.00	0.00	0.00	0.00	0.00
x_{1w} (Å)[a]	21.25	17.20	14.85	13.00	11.80	9.62	8.37
x_{2w} (Å)[a]	∞	39.00	31.00	29.00	26.60	26.55	27.70
x_{3w} (Å)		90.00	45.40	40.00	∞	47.70	33.80
x_{4w} (Å)		∞	52.20	*c*	*c*	*c*	*c,d*
x_{5w} (Å)			∞	∞	NA[f]	∞	∞
$P_{r,J}$	(>0.03)	(>0.60)	1.00	1.00	(>0.24)	0.60	0.50
e_w (%)[b]	53.44	38.58	5.86	3.30	13.87	5.38	1.42
x_0 (Å)	0.00	0.00	0.00	0.00	0.00	0.00	0.00
x_{1f} (Å)[a]	20.15	15.15	13.90	12.20	11.45	9.10	7.68
x_{2f} (Å)[a]	∞	40.70	31.90	32.55	28.80	31.50	30.20
x_{3f} (Å)		42.00	54.00	36.00	∞	55.00	43.40
x_{4f} (Å)		∞	60.50	*c*	*c*	*c*	*c,d*
x_{5f} (Å)			∞	∞	NA	∞	∞
$P_{r,opt}$	(>0.03)	(>0.60)	1.00	1.00	(>0.24)	0.60	0.50
e_f (%)[b]	53.11	40.02	1.33	1.00	15.27	1.02	0.08
$e^{(1,0.3)}$ (%)[e]	28.06	48.89	42.50	25.22	24.66	14.02	14.32
$e^{(1,1.0)}$ (%)[e]	28.06	48.89	37.91	19.94	24.66	6.06	6.92

[a] x_{1w} and x_{2w} are the lower and upper cutoff pore size limits from the pore volume distribution curves, and $x_{1,f}$ and $x_{2,f}$ are the corresponding limits from the $f(x)$ curves. [b] $e_{(W/f)} = 100\% \times (W_{calc,(W/f)} - W_{exp})/W_{exp}$, where W_{exp} and $W_{calc,(W/f)}$ are the measured and predicted total pore volumes, respectively. Predicted values are obtained from eq 8 with J equal to the corresponding segment number and the appropriate cutoff limits (on either the W or the f basis, see the previous point). [c] Heavy alkanes exhibit the same behavior in segments *iii* and *iv*; thus, segment *iii* is extended to also cover segment *iv*. [d] Segment *v* for *n*-heptane starts at $P_r = 0.5$ instead of 0.6. [e] $e^{(1,0.3)}$ and $e^{(1,1.0)}$ are the relative errors (defined as in note b) in predicting the total pore volumes from the one-segment Gaussian pore size distributions and experimental isotherms truncated at P_r of 0.3 and 1.0, respectively. [f] NA = No available experimental data in the corresponding segment.

in Figure 4 reveal that the resulting PSD may depend on the adsorbate, although in theory it should not. Nevertheless, all three potential theory models predicted similar average pore sizes, in fair agreement with DFT; however, only the multisegment approach gave a more realistic, but still only qualitative, view of the highly skewed PSD obtained from DFT. From a more positive point of view, these results also suggest that the potential theory methods can be used to predict the total pore volume of an adsorbent with reasonable accuracy, especially the new multisegment approach.

Conclusions

A very extensive set of single-component adsorption equilibria for the *n*-alkane series C_1−C_7 on Westvaco BAX-1100 activated carbon was measured over very broad ranges of temperature and pressure. A potential theory model correlated well with all of the data, and essentially a single characteristic curve was obtained that can be used to predict the adsorption equilibria of this *n*-alkane series on BAX-1100 activated carbon over a wide range of industrially relevant conditions. A simple functional form of the characteristic curve was found and provided for this purpose. This extensive data should also prove to be useful for evaluating the correlative ability of other adsorption isotherm models over a broad range of conditions. Some of these models can then be used to predict derived thermodynamic properties, such as the isosteric heat of adsorption and the adsorbed-phase heat capacity, that are difficult to measure. Part 2 of this series deals with this matter.

A new potential theory approach, based on a multisegment Gaussian distribution, was also developed and used to predict the total pore volume and pore size distribution of the BAX-1100 activated carbon from each of the *n*-alkanes. The results for the total pore volume compared favorably with that predicted from density functional theory, especially for the C_3−C_7 alkanes. However, the results for the PSDs were at best only qualitative, even for the C_3−C_7 alkanes. Nevertheless, the predictions were better than those obtained on the basis of a one-segment Gaussian distribution approach suggested in the literature. In fact, the results from the new approach can be used to more accurately examine the pore-filling pressure ranges of the *n*-alkanes C_3−C_7 because this new multisegment approach resulted in a skewed pore size distribution for the heavier *n*-alkanes that actually mimicked the multinodal pore size distribution from density functional theory. It is not possible to obtain a skewed distribution from the one-segment Gaussian approach. This extensive data set should also be useful for testing other adsorbent characterization schemes based on potential theory and other models.

Finally, this data set should prove to be very useful for predicting the behavior of hydrocarbon separation and purification processes, using BAX-1100 activated carbon as the adsorbent. It should prove to be especially useful for predicting the nonisothermal behavior of these processes, because the adsorption process models can be applied over very broad ranges of temperature and pressure (and thus loading) without resorting to extensive extrapolation of the data. The isosteric heats of adsorption and adsorbed-phase heat capacities that can be used in modeling the nonisothermal behavior of these systems are evaluated in Part 2 of this series.

Acknowledgment

The authors gratefully acknowledge financial support from the National Science Foundation under Grant CTS-9500362, the Westvaco Charleston Research Center, and the Separations Research Program at the University of Texas at Austin.

Supporting Information Available: Complete set of tabulated data for the experimental adsorption equilibria of the C_1−C_7 *n*-alkane series on BAX-1100 activated carbon. This material is available free of charge via the Internet at http://pubs.acs.org.

Literature Cited

(1) Jaroniec, M.; Madey, R. *Physical Adsorption on Heterogeneous Solids*; Elsevier: New York, 1988.

(2) Rudzinski, W.; Everett, D. H. *Adsorption of Gases on Heterogeneous Surfaces*; Academic Press: London, 1992.

(3) Masel, R. I. *Principles of Adsorption and Reaction on Solid Surfaces*; John Wiley and Sons: New York, 1996.

(4) Olivier, J. P. Characterization of Energetically Heterogeneous Surfaces from Experimental Adsorption Isotherms. In *Surfaces of Nanoparticles and Porous Materials*; Schwarz, J. A., Contescu, C. I., Eds.; Marcel Dekker: New York, 1999.

(5) Sircar, S. Isosteric Heats of Multicomponent Gas Adsorption on Heterogeneous Adsorbents. *Langmuir* **1991**, *7*, 3065.

(6) Ritter, J. A.; Al-Muhtaseb, S. A. New Model that Describes Adsorption of Laterally Interacting Gas Mixtures on Random Heterogeneous Surfaces. 1. Parametric Study and Correlation with Binary Data. *Langmuir*. **1998**, *14*, 6528.

(7) Sircar, S.; Rao, M. B. Heat of Adsorption of Pure Gas and Multicomponent Gas Mixtures on Microporous Adsorbents. In

Surfaces of Nanoparticles and Porous Materials; Schwarz, J. A., Contescu, C. I., Eds.; Marcel Dekker: New York, 1999; p.p. 501−528.

(8) Al-Muhtaseb, S. A.; Ritter, J. A. Roles of Surface Heterogeneity and Lateral Interactions on the Isosteric Heat of Adsorption and Adsorbed Phase Heat Capacity. *J. Phys. Chem. B.* **1999**, *103*, 2467−2479.

(9) Al-Muhtaseb, S. A.; Holland, C. E.; Ritter, J. A. Adsorption of C_1−C_7 Normal Alkanes on BAX Activated Carbon. 2. Deriving Thermodynamic Properties from the Adsorption Isotherms Using a Statistically Optimized Approach. *Ind. Eng. Chem. Res.*, in press.

(10) Szepesy, L.; Illes, V. Adsorption of Gases and Gas Mixtures. I. Measurement of the Adsorption Isotherms of Gases on Active Carbon up to Pressures of 1000 Torr. *Acta Chim. Hung. Tomus* **1963**, *35*, 37.

(11) Szepesy, L.; Illes, V. Adsorption of Gases and Gas Mixtures. II. Measurement of the Adsorption Isotherms of Gases on Active Carbon Under Pressures of 1 to 7 ATM. *Acta Chim. Hung. Tomus* **1963**, *35*, 53.

(12) Szepesy, L.; Illes, V. Adsorption of Gases and Gas Mixtures. III. Investigation of the Adsorption Equilibria of Binary Gas Mixtures. *Acta Chim. Hung. Tomus* **1963**, *35*, 245.

(13) Lastoskie, C.; Gubbins, K. E.; Quirke, N. Pore Size Distribution Analysis of Microporous Carbon: A Density Functional Theory Approach. *J. Phys. Chem.* **1993**, *97*, 4786.

(14) Lee, T. V.; Huang, J. C.; Rothstein, D.; Madey, R. Correlation of Adsorption Isotherms of Hydrocarbon Gases on Activated Carbon. *Carbon* **1984**, *22* (6), 493.

(15) Mehta, S. D.; Danner, R. P. An Improved Potential Theory Method for Predicting Gas-Mixture Adsorption Equilibria. *Ind. Eng. Chem. Fundam.* **1985**, *24* (3), 325.

(16) Chen, W.; Yang, R. T. Adsorption of Gas Mixtures and Modeling Cyclic Processes for Bulk, Multicomponent Gas Adsorption. *Recent Developments in Separation Science*; Li, N. N., Calo, J. M., Eds.; CRC Press: Boca Raton, FL, 1986; Vol. IX, Chapter 7, pp 135.

(17) Agrawal, R. K.; Schwarz, J. A. Analysis of High-Pressure Adsorption of Gases on Activated Carbon by Potential Theory. *Carbon* **1988**, *26* (6), 873.

(18) Dubinin, M. M. The Potential Theory of Adsorption of Gases and Vapors for Adsorbents with Energetically Nonuniform Surfaces. *Chem. Rev.* **1960**, *60*, 235.

(19) Reucroft, P. J.; Patel, K. B.; Chiou, C. T. Pore Volume Determination in Activated Carbon and Coal. *Carbon* **1982**, *22* (1), 100.

(20) Dubinin, M. M. Generalization of the Theory of Volume Filling of Microporous to Nonhomogeneous Microporous Structures. *Carbon* **1985**, *23* (4), 373.

(21) McEnaney, B. Estimation of the Dimensions of Micropores in Active Carbons Using the Dubinin−Radushkevich Equation. *Carbon* **1987**, *25* (1), 69.

(22) Carrott, P. J. M.; Roberts, R. A.; Sing, K. S. W. A New Method for the Determination of Micropore Size Distributions. In *Characterization of Porous Solids*; Unger, K. K., Rouquerol, J., Sing, K. S. W., Kral, H., Eds.; Elsevier Science Publishers: Amsterdam, 1988, pp 89.

(23) Jaroniec, M.; Lu, X.; Madey, R.; Choma, J. Comparative Studies of the Overall Adsorption Isotherm Associated with the Dubinin−Astakov Equation. *Carbon* **1990**, *28* (1), 243.

(24) Seifert, J.; Emig, G. Studies of the Microstructure of Porous Solids by Physisorption Measurements. *Int. Chem. Eng.* **1991**, *31* (1), 29.

(25) Jagiello, J.; Schwarz, J. A. Energetic and Structural Heterogeneity of Activated Carbons Determined Using Dubinin Isotherms and an Adsorption Potential in Model Micropores. *J. Colloid Interface Sci.* **1992**, *154* (1), 225.

(26) Nirmalakhandan, N. N.; Speece, R. E. Prediction of Activated Carbon Adsorption Capacities for Organic vapors Using Quantitative Structure−Activity Relationships Methods. *Environ. Sci. Technol.* **1993**, *27* (8), 1512.

(27) Aharoni, C.; Romm, F. A New Series of Equations for the Adsorption Isotherm Curves on Microporous Adsorbents. *Langmuir* **1995**, *11*, 1744.

(28) Chen, S. G.; Yang, R. T. Theoretical Investigation of Relationships Between Characteristic Energy and Pore Size for Adsorption in Micropores. *J. Colloid Interface Sci.* **1996**, *177*, 298.

(29) Burevski, D. Structural and Energetic Heterogeneities of Microporous Active Carbons. *Carbon* **1997**, *35* (7), 1001.

(30) Henley, E. J.; Seader, J. D. *Equilibrium-Stage Separation Operations in Chemical Engineering*; John Wiley and Sons: New York, 1981.

(31) Welty, J. R.; Wicks, C. E.; Wilson, R. E. *Fundamentals of Momentum, Heat, and Mass Transfer*, 3rd ed.; John Wiley and Sons: New York, 1984.

Received for review May 10, 2000
Accepted September 6, 2000

IE0004794